the FEBS Journal

Structural study of the catalytic domain of PKCζ using infrared spectroscopy and two-dimensional infrared correlation spectroscopy

Sonia Sánchez-Bautista, Andris Kazaks*, Melanie Beaulande, Alejandro Torrecillas, Senena Corbalán-García and Juan C. Gómez-Fernández

Departamento de Bioquímica y Biología Molecular, Universidad de Murcia, Spain

Keywords
2D-correlation; catalytic domain; FTIR; protein kinase C; protein structure

Correspondence
J. C. Gómez-Fernández, Departamento de Bioquímica y Biología Molecular (A), Facultad de Veterinaria, Universidad de Murcia, Apartado de Correos 4021, E-30080 Murcia, Spain
Fax: +34 968 36 4766
Tel: +34 968 36 4766
E-mail: jcgomez@um.es

***Present address**
Biomedical Research and Study Centre, University of Latvia, Riga, Latvia

(Received 27 January 2006, revised 22 May 2006, accepted 23 May 2006)

doi:10.1111/j.1742-4658.2006.05338.x

The secondary structure of the catalytic domain from protein kinase C ζ was studied using IR spectroscopy. In the presence of the substrate MgATP, there was a significant change in the secondary structure. After heating to 80 °C, a 14% decrease in the α-helix component was observed, accompanied by a 6% decrease in the β-pleated sheet; no change was observed in the large loops or in 3_{10}-helix plus associated loops. The maximum increase with heating was observed in the aggregated β-sheet component, with an increase of 14%. In the presence of MgATP, and compared with the sample heated in its absence, there was a substantial decrease in the 3_{10}-helix plus associated loops and an increase in α-helix. Synchronous 2D-IR correlation showed that the main changes occurred at 1617 cm^{-1}, which was assigned to changes in the intermolecular aggregated β-sheet of the denaturated protein. This increase was mainly correlated with the change in α-helix. In the presence of MgATP, the main correlation was between aggregated β-sheet and the large loops component. The asynchronous 2D-correlation spectrum indicated that a number of components are transformed in intermolecularly aggregated β-sheet, especially the α-helix and β-sheet components. It is interesting that changes in 3_{10}-helix plus associated loops and in α-helix preceded changes in large loops, which suggests that the open loops structure exists as an intermediate state during denaturation. In summary, IR spectroscopy revealed an important effect of MgATP on the secondary structure and on the thermal unfolding process when this was induced, whereas 2D-IR correlation spectroscopy allowed us to show the establishment of the denaturation pathway of this protein.

Protein kinase C (PKC) is a family of related protein kinases that plays an important role in regulating cell growth. These protein kinases are involved in several intracellular pathways that end in transcription and are considered to be potential targets for anticancer therapy [1,2]. PKCs include at least 10 different mammalian isoforms that can be classified into three groups according to their structure and cofactor regulation. The first group includes the classical PKC isoforms (α, βI, βII and γ), which are regulated by acidic phospholipids, diacylglycerol, phorbol esters and also by calcium. The second group corresponds to the novel PKC isoforms (δ, ε, η and θ), which are regulated by phospholipids, diacylglycerols and phorbol esters but not by calcium. The third group comprises the atypical PKC isoforms (ζ, τ/L and μ), which are not regulated

Abbreviations
cat-ζ, catalytic domain from PKCζ; PKC, protein kinase C; PKCζ-kn, kinase-defective dominant-negative form of PKCζ; PS, pseudosubstrate; $PtdInsP_3$, phosphatidylinositol 3,4,5-triphosphate.

by diacylglycerol or by calcium [3,4] but are directly or indirectly activated by phosphatidylinositol 3,4,5-trisphosphate ($PtdInsP_3$) [5,6] and other lipids, such as ceramides and arachidonate [7], and phosphatidic acid [8]. Like other atypical isoenzymes, PKCζ, consists of four functional domains and motifs, including a PB1 domain in the N-terminus, a pseudosubstrate (PS) sequence, a C1 domain of a single Cys-rich zinc-finger motif, and a kinase domain in the C-terminus. The catalytic region is relatively similar to those of the remaining PKC isoenzymes, although their regulatory regions are clearly different because they do not have a C2 domain and the C1 domain is atypical with respect to the classical and novel isoenzymes and is not sensitive to diacylglycerol or phorbol esters.

The kinase domain of PKCζ, as well as other members of the AGC group, includes an MgATP-binding region, an activation loop, a turn motif and a hydrophobic motif. The MgATP-binding region contains a Lys residue, Lys281, which is crucial for its kinase activity. A mutant whose Lys281 is substituted by other amino acids is usually used as a kinase-defective dominant-negative form of PKCζ (PKCζ-kn). Whereas classical and novel isoforms of PKC have three phosphorylation sites localized in the activation loop, the turn motif and the hydrophobic motif, PKCζ has only two phosphorylation sites, namely residues T410 (in the activation loop) and T560 (in the turn motif) which are phosphorylated upon activation [9,10]. However, no phosphorylated residue has been detected in the hydrophobic motif of the atypical PKCs [11].

PKCs have been shown to play an essential role in a wide range of cellular functions including mitogenic signalling, cytoskeleton rearrangement, glucose metabolism, differentiation, and the regulation of cell survival and apoptosis [12–15]. Many of these cellular functions are related to human diseases and PKC inhibitors are currently being used in clinical trials for various types of cancer, and a PKCβ inhibitor is being used in trials for diabetes-related retinopathy [16].

PKCζ is a member of the atypical PKC subfamily and has been widely implicated in the regulation of cellular functions. Increasing evidence from studies using *in vitro* and *in vivo* systems points to PKCζ as a key regulator of the critical intracellular signalling pathways that are induced by various extracellular stimuli, and this enzyme has been implicated in several types of cancer [11,17]. For this reason it is of great interest to study the structure of the catalytic domain of PKCζ and its interaction with substrates.

To date, no full structure of a complete PKC isoform, at an atomic resolution level, has been described, although the structures of isolated regulatory domains of some classical and novel PKC isoenzymes are known, and the structure of the catalytic domain of an atypical PKC (PKCι) has recently been reported [18]. The overall structure exhibits the classical bilobal kinase fold, with both phosphorylation sites (Thr403 in the activation loop and Thr555 in the turn motif) well defined in the structure, and forming intramolecular ionic contacts. These make an important contribution to stabilizing the active conformation of the catalytic subunit. The structure of the first catalytic domain of a novel PKC, as PKCθ is, has also been recently solved at high resolution [19].

In this study we used IR spectroscopy to study the secondary structure of the catalytic domain of PKCζ and the effect of its substrate, MgATP, and also to study the effect of thermal unfolding in the presence and the absence of MgATP. We used 2D correlation spectroscopy to gain information into the correlation between different elements of the secondary structure during denaturation. The results showed an important effect of MgATP on the secondary structure and on the thermal unfolding process when this was induced.

Results

Information on the secondary structure of the catalytic domain from PKCζ (cat-ζ) was obtained by analysis of the IR amide I band, located between 1700 and 1600 cm^{-1} and arising mainly from the C = 0 stretching vibration of the peptidic bond. This band is conformationally sensitive and can be used to monitor either the secondary structure composition or changes induced in the protein by external agents [20]. Spectra were obtained using H_2O and D_2O buffers, and the spectra shown were obtained by subtracting the spectra of buffers and ligands (like MgATP) from those of samples containing protein. Figure 1A shows the difference spectra of cat-ζ in the presence of D_2O buffer (5 $mg{\cdot}mL^{-1}$). The spectra of protein samples, prepared in D_2O buffer, are also shown at 80 °C, and in the presence of the enzyme substrate MgATP at 25 and 80 °C.

To better appreciate the effect of heating on the protein structure, difference spectra were obtained by spectra subtraction (Fig. 1A). More specifically, Fig. 1B shows the difference between the spectrum of cat-ζ obtained in D_2O buffer at 25 °C and the same sample at 80 °C. It can be seen that heating induced a very substantial increase at 1616 and 1683 cm^{-1}, and a very substantial decrease in the region 1660–1630 cm^{-1}, with a maximum within this region, at 1657 cm^{-1}. The meaning of these variations is discussed below. Also interesting was the effect of heating

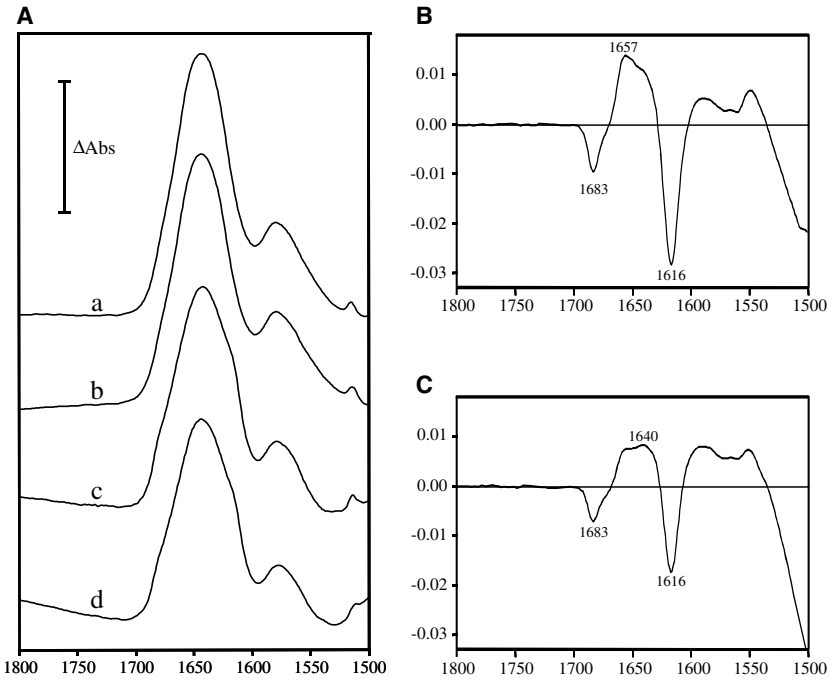

Fig. 1. FTIR spectra of cat-ζ in D_2O buffer at 25 °C. The protein concentration was 5 mg·mL^{-1} (105 μM). The increase in absorbance units (ΔAbs) was 0.04. (A) FTIR spectra in the range between 1800 and 1500 cm^{-1}, where the amide I′ and amide II regions can be observed for (top to bottom) cat-ζ at 25 °C (a), cat-ζ at 25 °C plus 1 mM MgATP (b), cat-ζ at 80 °C (c) and cat-ζ at 80 °C in the presence of 1 mM MgATP (d). In all cases, the spectrum shown was obtained by subtracting the buffer spectrum, which also contained MgATP in cases (b) and (d). (B) The difference spectrum obtained by subtracting (c) from (a). (C) The difference spectrum obtained by subtracting (d) from (b). In order to obtain difference spectra (B) and (C) subtraction of the two absorption spectra was performed by using a factor that led to the 1700–1600 cm^{-1} interval (amide I) having the same positive and negative area.

in the presence of MgATP, which can be seen after obtaining the spectrum of cat-ζ at in D_2O buffer at 25 °C and subtracting the spectrum of the same sample at 80 °C. Figure 1C shows a very considerable increase upon heating at 1616 and 1683 cm^{-1}, whereas a decrease was observed in the region 1660–1630 cm^{-1} although, unlike the situation in the absence of MgATP, the maximum was now located at 1640 cm^{-1}. This indicated that the different types of secondary structure were not equally protected from denaturation by the presence of MgATP, as is shown in detail after decomposition of the amide I band.

Figure 2 shows the spectrum obtained in H_2O buffer in the absence of ligands at 25 °C (20 mg·mL^{-1}). In order to decompose the amide I band, the number and initial positions of the component bands were obtained from band-narrowed spectra by derivation (Fig. 2B). Amide I band decomposition of cat-ζ H_2O at 25 °C is shown in Fig. 2C. The corresponding parameters, i.e. band position, percentage area and assignment, are shown in Table 1.

The spectrum in H_2O showed seven components in the amide I region. The main component, which accounted for 43% of the total band area, was localized at 1657 cm^{-1} and can be assigned to an α-helix although it may also arise from a disordered structure [20]. Because these two types of structure are not distinguished when using H_2O buffer, it is convenient to inspect the spectrum obtained in D_2O buffer. The component found at 1631 cm^{-1} (14%) can be assigned to a β structure [20]. The components appearing at 1672 cm^{-1} (9%), 1681 cm^{-1} (7%) and 1691 cm^{-1} (3%) may arise from β-turns [21,22], although the last two may also arise in part from β-sheet [20,23]. Another component was located at 1641 cm^{-1} (19%) and can be assigned to loops or a 3_{10}-helix [23]. However, taking into account the spectrum decomposition of the amide I′ band obtained in D_2O buffer, as shown below, we assigned it to both. Finally, another component band appeared at 1622 cm^{-1} (5%). This has usually been attributed to peptides in an extended configuration with a hydrogen-bonding pattern formed by peptide residues not taking part in the intramolecular β-sheet, but rather hydrogen-bonded to other molecular structures [20,24,25]. Nevertheless, this frequency when associated with another peak at 1693 cm^{-1}, both in H_2O and D_2O, has been attributed to β-hairpin [26]. Note that we observed a band at 1691 cm^{-1} (Table 1), and it might be possible to assign this component to β-hairpin at 25 °C. It should also be noted that the area located between 1600 and 1615 cm^{-1}, which corresponds to contributions of aminoacyl side chains, was not taken into account.

When spectra were obtained in the presence of D_2O buffer for a sample of cat-ζ at 25 °C (Fig. 1A) it was seen that the amide II band observed in samples prepared in the presence of H_2O buffer and centred at ~1560 cm^{-1} decreased very considerably as a

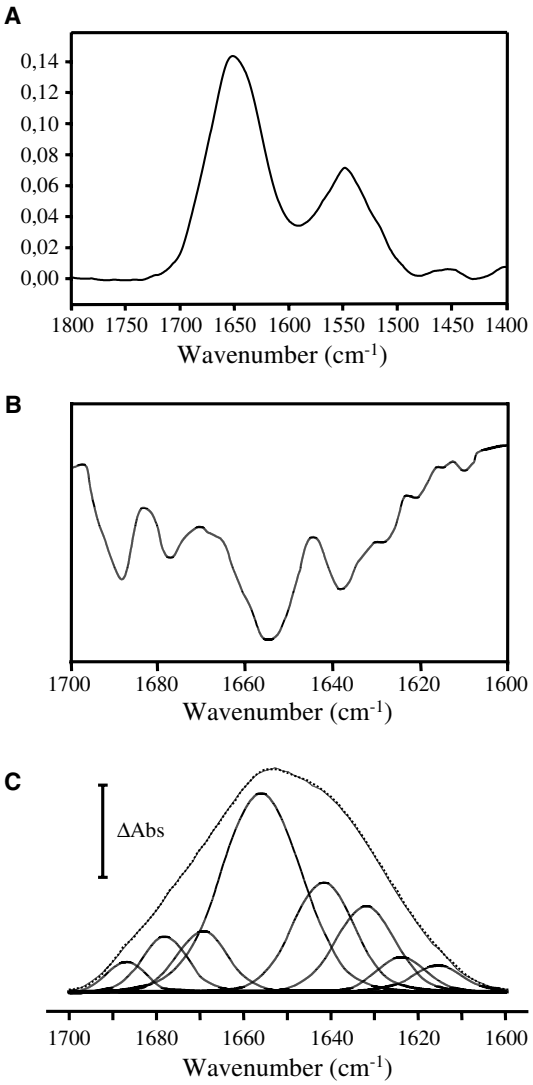

Fig. 2. FTIR spectra of cat-ζ in H_2O buffer at 25 °C. The protein concentration was 20 mg·mL^{-1} (421 μM). The vertical bar (ΔAbs) represents 0.05 absorbance units. (A) FTIR difference spectrum obtained by subtracting the spectrum of the solvent from the spectrum of the protein in the same solvent, in the range 1800–1500 cm^{-1}, where the amide I and amide II regions can be observed. (B) Second derivative of the FTIR spectrum of this sample. (C) FTIR spectrum (solid line) in the amide region with the fitted component bands. The parameters corresponding to the component bands are shown in Table 1. The dashed line represents the curve-fitted spectrum, i.e. the dotted line is the sum of the individual components.

consequence of the use of D_2O buffer. This is the consequence of the H–D exchange that takes place when using D_2O buffer, a range of that was quantified using two different procedures. The first implied calculating the ratio between the areas of the amide II and amide I bands [27] when the exchange was found to be 83.8% in the presence of D_2O buffer. This percentage seems to be related to maximum exchange because, after heating at 80 °C, i.e. after thermal denaturation, the percentage exchange increased, but only very slightly to 85.7%. Similar percentages were also obtained in the presence of MgATP. The second procedure consisted of obtaining the ratio between the absorbance values at 1550 (amide II) and at 1515 cm^{-1}, which corresponds to tyrosine (Fig. 1A). The band at 1515 cm^{-1} was used to normalize the data because it was not affected by the H–D exchange [28]. The ratios obtained from the samples studied in D_2O buffer were then compared with those obtained in the presence of H_2O buffer. The results were very similar to those found using the first procedure with a percentage exchange of 89.8% at 25 °C and 93.3% at 80 °C, confirming that heating at 80 °C did not appreciably enhance H–D exchange. Similar percentages were also obtained when this procedure was used in the presence of MgATP.

The amide I′ band of cat-ζ in D_2O at 25 °C was decomposed using the same procedure described above for samples in the presence of H_2O buffer (Fig. 2). The corresponding parameters, i.e. band position, percentage area and assignment, are shown in Table 1. The spectra in D_2O showed eight component bands in the 1700–1600 cm^{-1} region and the quantitative contribution of each band to the total amide I′ contour was obtained by band curve fitting of the original spectra. The major component in the amide I′ region appears at 1658 cm^{-1} (27%), which can be assigned to α-helix [20,23,29,30] and is separated from a component appearing in this D_2O buffer at 1648 cm^{-1} (16%), which has been attributed to large open loops, i.e. fully hydrated, not interacting with proximate amide functional groups [20,23].

The high-frequency components at 1669 cm^{-1} (8%), 1679 cm^{-1} (6%) and 1689 cm^{-1} (1%) can be assigned to β-turns and the last two also partially to β-sheet [23]. It was predicted that the high-frequency component intensity is less than 1/10th that of the low-frequency band, appearing at 1631 cm^{-1}, and amounting to 17% [31]. The high-frequency components are attributed to the antiparallel β-sheet structure [30,32] appearing at 1679 and 1689 cm^{-1} in D_2O buffer and 1681 and 1691 cm^{-1} H_2O. The component appearing at 1622 cm^{-1} (7%) was not shifted by the H–D exchange, which is compatible with its origin in intermolecular β-sheet or from β-hairpin. Finally, the 1641 cm^{-1} component was shifted only 1 cm^{-1} with respect to that observed in H_2O buffer, strongly suggesting that it arises from a 3_{10}-helix or perhaps from associated loops which therefore have a low accessibility to D_2O exchange.

Table 1. FTIR parameters of the amide I band components of cat-ζ (20 mg·mL^{-1}) in H_2O buffer or cat-ζ (5 mg·mL^{-1}) in D_2O buffer at 25 *C and in the absence or presence of ATP.

	H_2O (25 °C)		D_2O (25 °C)		D_2O+ATP (25 °C)		D_2O (80 °C)		D_2O+ATP (80 °C)	
Assignment	position[a] (cm^{-1})	area[b] (%)	position (cm^{-1})	area (%)	position (cm^{-1})	area (%)	position (cm^{-1})	area (%)	position (cm^{-1})	area (%)
β-turns+ β-sheet	1691	3	1689	1	1688	1	1680	8	1681	6
β-turns+ β-sheet	1681	7	1679	6	1678	7	1667	13	1673	6
β-turns	1672	9	1669	8	1669	7			1664	11
β-turns							1657	13	1655	18
α-helix	1657	43	1658	27	1659	23	1649	16	1647	15
Open loops			1648	16	1648	23	1640	18	1639	13
3_{10}-helix + associated loops	1641	19	1640	18	1640	11	1632	11	1632	10
β-sheet	1631	14	1631	17	1631	23	1620	21	1621	21
Intermolecular β-sheet + β-hairpins	1622	5	1622	7	1621	5				

[a] Peak position of the amide I band components. [b] Percentage area of the amide I band components. The area corresponding to side chain contributions located at 1600–1615 cm^{-1} has not been considered.

To be activated, PKCζ, must be phosphorylated in the catalytic domain [11]. We verified that cat-ζ was phosphorylated from the observation that the PO_2^- double-bond asymmetric stretching band appeared at 1244 cm^{-1} [33] in the spectrum taken in H_2O buffer and in the total absence of MgATP (not shown for the sake of brevity).

When the effect of ligands such as the pseudosubstrate peptide (see Experimental procedures) and MgATP on the secondary structure of cat-ζ was tested, only MgATP induced changes in the secondary structure, an observation that can be considered significant. Table 1 shows that in D_2O buffer the presence of MgATP induced a 4% decrease in the α-helix structure appearing at 1659 cm^{-1}, which decreased to 23%, and a 7% decrease in the component assigned to 3_{10}-helix plus associated loops at 1640 cm^{-1}, which decreased to 11%. However, the component absorbing at 1648 cm^{-1} (attributed to open loops) increased to 23% (a 7% increase), whereas in the β-sheet component at 1631 cm^{-1} it reached 23% (a 6% increase). It seems, then, that this substrate was able to modulate the secondary structure significantly.

To gain further insight into the structure and folding of cat-ζ and into the structural changes that occur during MgATP binding, thermal-stability studies were performed. The FTIR spectrum of cat-ζ in D_2O buffer revealed major changes in the amide I′ mode at 80 °C (Fig. 1A, Table 1). These included a broadening of the overall amide I′ contour and an increase in the area under the component at 1620–1621 cm^{-1}, which reached 21% (a 14% increase). This can be attributed to β-sheet with intermolecular bonds, which is characteristically important in thermally denatured proteins [32,34]. This component indicates that extended structures were formed by aggregation of the unfolded proteins produced as a consequence of irreversible thermal denaturation [34–36]. The increase in the components contrasted with a decrease in the α-helix component appearing at 1657–1658 cm^{-1}, which decreased to 13% (a decrease of 14%), and the β-pleated sheet, centred at 1631–1632 cm^{-1} which decreased to 11% (a decrease of 6%; Table 1). These observations agreed with the difference spectrum shown in Fig. 1B. The components appearing at 1648–1649 and 1640 cm^{-1} (attributed to large open loops and 3_{10}-helix plus associated loops, respectively) did not change significantly.

The presence of MgATP during the heating process did not prevent an increase in the area of the component considered characteristic of denaturated proteins, at 1621 cm^{-1}, which continued to be 21% (Table 1), and prevented changes in several other components. Of note is the fact that, with respect to the situation at 25 °C, and in the presence of MgATP, the α-helix component appearing at 1655–1659 cm^{-1} represented 18% of the total area, hence the decrease was only 5% (Table 1). In contrast, the 3_{10}-helix plus associated loops component (1639–1640 cm^{-1}) did not change significantly. The β-pleated sheet (1631–1632 cm^{-1}) also suffered a substantial decrease to 10% (a 13% decrease), whereas the component at 1647–1648 cm^{-1} attributed to exposed loops also decreased to 15% (representing a decrease of 8%). Again, these changes, including the preservation of the α-helix component in the presence of MgATP, agreed quite well with the difference spectrum shown in Fig. 1C.

Figure 3 shows a plot of the half-height width of the amide I′ band versus temperature, which is one way of

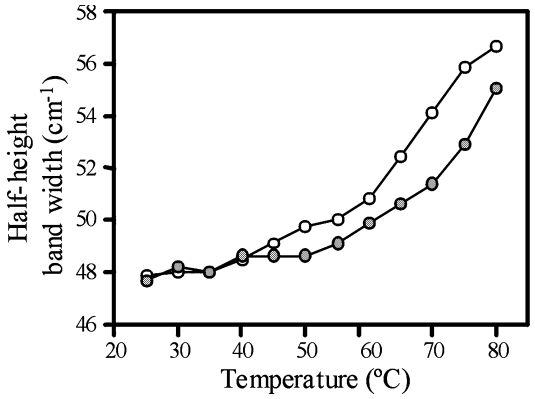

Fig. 3. Half-height bandwidth of the amide I′ region of the FTIR spectra in cm^{-1} as a function of temperature from 25 to 80 °C for the cat-ζ in D_2O buffer in the absence (○) or the presence of 1 mM MgATP (●).

following protein denaturation [29]. As can be seen, the onset of widening occurred at 40 °C in the absence of MgATP, but shifted to 50 °C in the presence of MgATP, indicating a protective effect by the substrate.

In order to better visualize the changes taking place during thermal denaturation, 3D spectra were constructed (Fig. 4). When the cat-ζ spectra obtained in the absence (Fig. 4A) and in the presence (Fig. 4B) of MgATP were compared the widening of the overall amide I′ contour was less in the presence of MgATP and the aggregation-indicative band at 1618 cm^{-1} could be clearly visualized.

2D-IR correlation studies

The above thermal profiles and curve-fittings cannot provide information on the interactions between the secondary-structure elements that give rise to the observed changes. Such interactions can, however, be monitored in detail using 2D-IR correlation spectroscopy. In a synchronous 2D map, peaks located along the diagonal (autopeaks) correspond to changes in intensity induced, in this case, by temperature, and they are always positive. Cross-correlation (nondiagonal) peaks indicate an in-phase relationship between the two bands involved, i.e. that two vibrations of the protein, characterized by two different wave numbers (ν_1 and ν_2) are being affected simultaneously [37]. A deeper insight into the mechanism of protein unfolding and the role of the different ligands was therefore obtained using 2D-IR correlation spectroscopy, a technique that we have previously used to study the thermal unfolding of C2 domains from classical PKCs [38] and also the full PKCα [39]. In all cases, the average spectra of the temperature scans from 25 to 80 °C were used as reference in the analysis.

The synchronous 2D-IR correlation contour map of cat-ζ in the absence of MgATP, corresponding to heating from 25 to 80 °C (Fig. 5A), shows two autopeaks

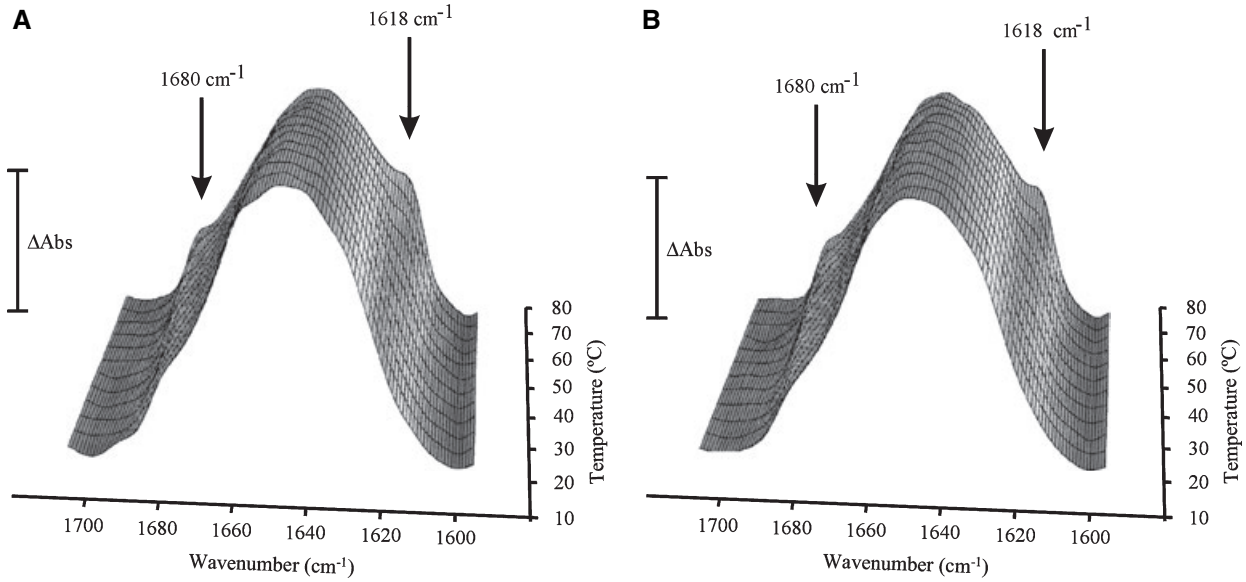

Fig. 4. Deconvolved FTIR spectra of cat-ζ in the amide I′ region (1700–1600 cm^{-1}) as function of temperature from 25 to 80 °C in the absence (A) or presence (B) of 1 mM MgATP. The protein concentration was 5 $mg \cdot mL^{-1}$ (105 μM). The bands indicating aggregation (1618 and 1680 cm^{-1}) are shown. The increase of absorbance units (ΔAbs) was 0.04.

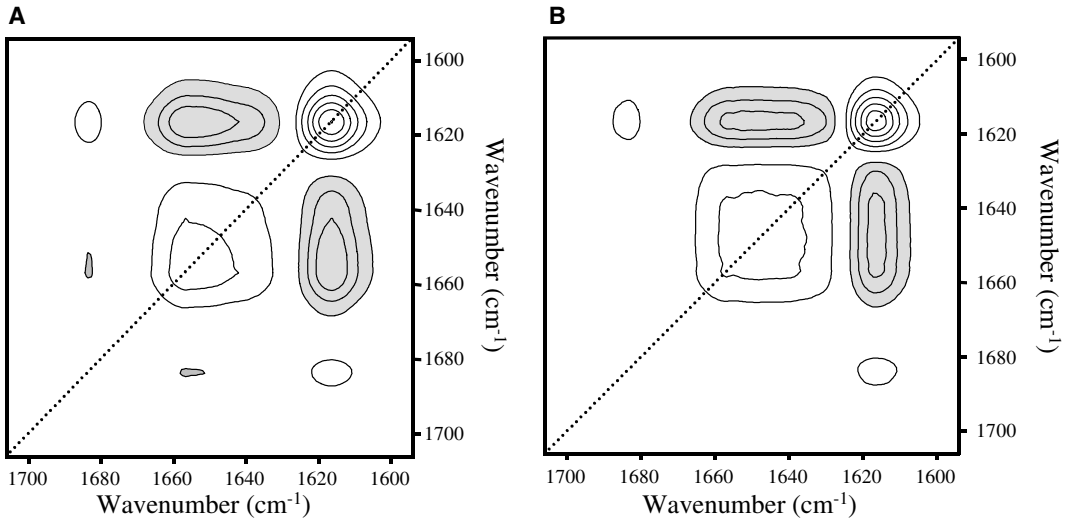

Fig. 5. Synchronous 2D-IR correlation spectra of the catalytic domain from PKCζ (cat-ζ) in D_2O buffer as a function of temperature variation between 25 and 80 °C in the absence (A) or presence (B) of ATP 1 mM. Correlation spectra were obtained using the 2D-POCHA program. White and dark peaks are positive and negative peaks, respectively.

located at 1617 and 1657 cm^{-1}, indicating that these are the frequencies at which the main changes take place during the thermally induced unfolding of the protein. The most intense cross-peaks were observed at the same frequencies (1617–1657 cm^{-1}) and were negative, indicating that during the heating process one increased as the other decreased. Less intense, but informative, cross-peaks were observed correlating 1684 and 1659 cm^{-1}. These were negative, indicating that the other component associated with denaturation also increased, whereas the α-helix decreased; however, quantitatively, this peak was smaller. In addition, positive cross-peaks were also observed correlating 1617 and 1684 cm^{-1}, indicating that these two components, which are associated during denaturation, were synchronized. These observations are fully consistent with the IR spectroscopic studies described above, emphasizing that the disappearance of the α-helix component is associated with the appearance of the intermolecularly aggregated β-sheet.

When the correlation was made in the presence of MgATP (Fig. 5B), there was a significant change in the synchronous contour map because the autopeaks were now centred at 1617 and 1648 cm^{-1}, indicating that the component which decreased due to denaturation was now the one assigned to large open loops. Negative cross-peaks correlated 1617 and 1652 cm^{-1}, indicating correlation between the decrease in this lower frequency α-helix or open loops and the increase in intermolecularly aggregated β-sheet. The correlation observed at 1652 cm^{-1}, a frequency at which no component was found during amide I′ decomposition, may indicate that spectral widening is taking place [40], as occurs during denaturation. Finally, a small positive peak correlated 1617 and 1684 cm^{-1}, and this again may be interpreted as the simultaneous increase in these two components, both of which are associated with protein denaturation.

The asynchronous 2D-IR correlation contour maps of cat-ζ in the absence and presence of MgATP due to the thermal denaturation from 25 to 80 °C are shown in Fig. 6. Figure 6A shows the results in the absence of MgATP and reveals a number of correlations between 1614 and 1616 cm^{-1} and several other components. There is a correlation cross-peak at 1614–1683 cm^{-1} with a negative sign, indicating that the increase at 1683 cm^{-1} preceded that at 1614 cm^{-1}. The correlation cross-peak at 1614–1659 cm^{-1} is positive, but was found in an area with a negative sign in the corresponding synchronous map, so that the change at 1659 cm^{-1} occurred before that at 1614 cm^{-1}. Similar situations occurred with the correlation cross-peak located at 1614–1649 cm^{-1}, which had a positive sign, meaning that the change at 1649 cm^{-1} preceded that at 1614 cm^{-1}, and with the correlation cross-peak at 1614–1642 cm^{-1}, the change at 1642 cm^{-1} once again preceding that at 1614 cm^{-1}.

Other correlation asynchronous cross-peaks with positive signs were observed, such as that correlating 1653 and 1684 cm^{-1}, indicating that the change at 1653 preceded that at 1684 cm^{-1}, and the cross-peak correlating 1642 and 1653 cm^{-1}, such that the change

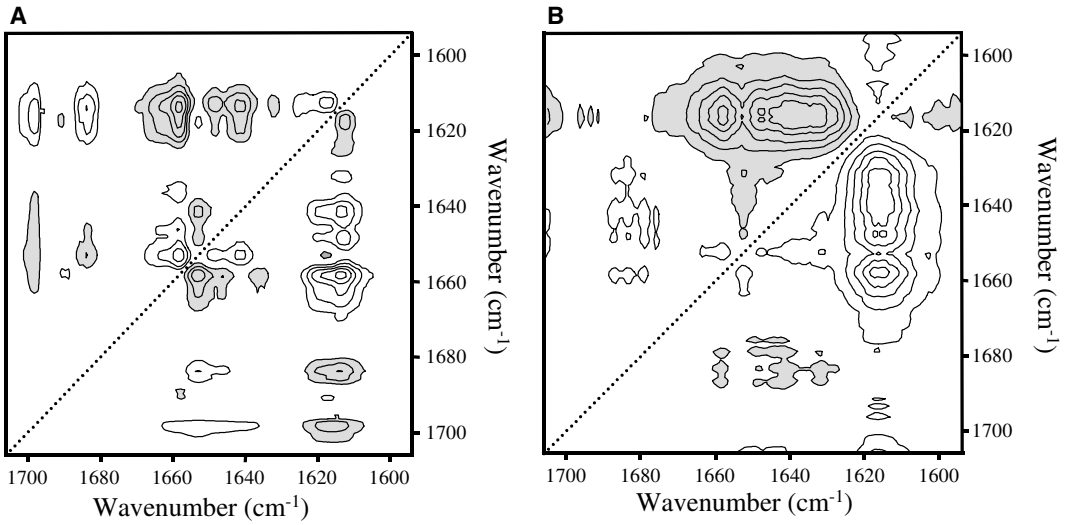

Fig. 6. Asynchronous 2D-IR correlation spectra of the catalytic domain from PKCζ (cat-ζ) in D_2O buffer as a function of temperature variation between 25 and 80 °C in the absence (A) or presence (B) of 1 mM MgATP. Correlation spectra were obtained using the 2D-POCHA program. White and dark peaks are positive and negative peaks, respectively.

in the component at 1642 cm^{-1} occurred before that at 1653 cm^{-1}. Finally, there was a peak signalling a correlation between 1653 and 1658 cm^{-1}, which has a negative sign and therefore indicates that the change at 1658 cm^{-1} precedes that at 1653 cm^{-1}. The butterfly form of these correlation peaks indicates the existence of a shift in frequencies associated with denaturation, so that the α-helix component is being transformed in the large open loops structure occurring at 1648 cm^{-1}.

In the presence of MgATP (Fig. 6B) the asynchronous correlation map again correlates the 1617 cm^{-1} component with 1658, 1647 and 1640 cm^{-1}, all with a positive sign, although the corresponding area in the synchronous map was negative. Therefore, changes at 1617 cm^{-1} occurred after changes in the other components, probably indicating that all decrease during denaturation, leading to the appearance of the 1617 cm^{-1} component associated with intermolecularly aggregated β-sheet.

Discussion

The structure of PKCζ is not entirely known, nor is structure of its catalytic domain. However, two catalytic domains from other PKCs have been determined at high resolution, that of PKCι [18] (PDB code 1ZRZ) and that of PKCθ [19] (PDB code 1XJD), although this has been only partially determined because the structure of 282 residues of a total of 344 have been solved [19]. The catalytic domain of PKCθ possesses a high degree of homology (~ 80%) with the catalytic domain of other isoforms of PKC belonging to the classical or novel subfamilies. However, the percentage identity between the catalytic domain of PKCθ and cat-ζ is considerably lower (44%). It should be noted that the percentage sequence identity of cat-ζ with other kinases and with the catalytic domain of cAMP-activated protein kinase [41] (PDB code 1J3H) is only slightly lower, amounting to 39%. In the case of the catalytic domain of PKB [42] (PDB code 1MRV), the homology with cat-ζ is 48%, It is noticeable that for the catalytic domain of PKCι, the degree of sequence homology with that of PKCζ is ~84%, which is a consequence of the very early separation of the branch of the atypical PKCs from other protein kinases in the evolutionary tree [43].

It is, however, striking that, besides the lack of sequence homology, there is remarkable analogy in the 3D structures. The structure of the catalytic domain of PKCι [18] is similar to that of PKCθ [19] which, in turn, is similar to those of PKB [42] (PDB code 1MRV) and PKA [41] (PDB code 1J3H), formed by two lobes, a small N-lobe and a bigger C-lobe. MgATP binds between both lobes and establishes polar interactions with residues located in other lobes.

We studied the secondary structure of the catalytic domain of PKCζ, its denaturation properties and the effect of its substrate, MgATP, on the structure and denaturation properties. Comparison of the structure in H_2O buffer and D_2O buffer facilitated assignment of the various components detected using band-narrowing and band-fitting techniques. At 25 °C it was

Table 2. Comparison of the secondary structure of PKCζ with those from other protein kinases of the AGC family. The structures of protein kinases were taken from: PKA [41] (PDB code 1J3H), PKB inactive, i.e. apoenzyme [42] (PDB code 1MRV), PKB active, i.e. complexed with AMPPNP [44] (PDB code 1O6K); PKCι [18] (PDB code 1ZRZ and PKCζ (our data of the sample in D_2O at 25 °C without Mg^2 ± ATP). ND, not determined.

	PKA	PKB inactive	PKB active	PKCι	PKCζ
α-helix	31.4	21.1	28.3	25.6	27.0
β-pleated sheet	14.0	13.0	15.2	13.7	17.0
3_{10}-helix	3.4	4.4	2.7	3.3	ND
β-turns	15.2	13.9	17.0	13.2	15.0

concluded that the secondary structure included two types of helix, an α-helix absorbing at 1658 cm^{-1} and another whose presence may be inferred from the component absorbing at 1640 cm^{-1} to be an 3_{10}-helix. In addition, it should be noted that two types of loops may be present, one corresponding to open large loops which suffer a large frequency shift in the presence of D_2O (from 1657 to 1648 cm^{-1}) and the other corresponding to the component absorbing at 1640–1641 cm^{-1}, which hardly shifted when exposed to D_2O buffer. These assignments are compatible with the information available for other catalytic domains from protein kinases, such as cAMP-dependent protein kinase [41], PKB [44] or PKCι [18] and all contain 3_{10}-helix. However, the percentage of 3_{10}-helix in all these catalytic domains, which are analogous to that of PKCζ, is ~3–4% (Table 2) and so a substantial part of the 18% found in the sample at 25 °C (in the absence of MgATP) for the component centred at 1640 cm^{-1} (Table 1) can be assigned to loops, because there is a very small shift due to D_2O buffer (only 1 cm^{-1}), these loops must be interacting either with themselves or with other structures.

A number of authors have previously assigned components absorbing at 1640–1643 cm^{-1} in D_2O to 3_{10}-helices, for example, in the cases of cytochrome b_5 [45], alpha lactalbumin [46], streptokinase [23], short alanine-based peptides [47] and cytochrome P-450 [48] among others. Components absorbing at 1640–1643 cm^{-1} in D_2O have also been assigned to loops in streptokinase [23], photosystem II reaction centre [49] or acetylcholinesterase [50]. The spectrum in H_2O suggests that these loops are not very accessible to the solvent.

Comparison of the secondary structure of PKCζ with those of other protein kinases of the AGC family (Table 2) offers other interesting data. The secondary structure of PKCι, as deduced from the published 3D structure [18], is very similar to that of PKCζ, as concluded from our IR work, and although this is not unexpected given the high sequence homology, it lends weight to the reliability of IR-spectroscopy. Also of note, is the relatively high similarity in secondary structure observed for PKB and PKA with respect to PKCζ.

An interesting aspect of the catalytic domains of PKCθ is that it has been reported to possess four β-hairpins (see structure with PDB code 1XJD), whereas the structure of PKCι also showed four β-hairpins, amounting to ~7% of the total [18] (PDB code 1ZRZ). The 1622 cm^{-1} component, which is usually attributed to peptides in intramolecular hydrogen bonding [20,24,25], has also been assigned to β-hairpin when associated with another peak at 1693 cm^{-1} in both H_2O and D_2O [26]. Note that the band at 1691 cm^{-1} (Table 1) supports the occurrence of a β-hairpin structure. Whatever the case, the observed increase in this component upon heating may be attributed to the formation of intermolecular hydrogen bonded β-sheet which is associated with this process.

As mentioned above, thermal denaturation produced an increase in the 1620 cm^{-1} component, implying an increase in the width of the amide I′ band, although the main loss was observed in the 1657 cm^{-1} component. It is of note that the widening of the amide I′ band (Fig. 3) is not so pronounced as in other proteins, probably because the denaturation process is not very cooperative, at least between 40 and 60 °C. These changes were clearly revealed by the synchronous 2D correlation map, which indicated that the decrease in α-helix correlated with the increase in intermolecular hydrogen-bonded β-pleated sheet.

The asynchronous 2D correlation spectrum is compatible with the transformation of the secondary structure, so that a number of components are transformed into intermolecularly aggregated β-sheet, especially the α-helix and 3_{10}-helix plus associated loops and the β-sheet components.

Note that during thermal unfolding changes in 3_{10}-helix plus associated loops and in the α-helix preceded changes in the open large loops absorbing at 1648 cm^{-1}. These open loops act as an intermediate state preceding aggregated β-sheet, which may be correlated with the fact that during thermal unfolding there is no change in the percentage corresponding to large open loops, whereas there is a decrease in α-helix and in the component assigned to 3_{10}-helix plus associated loops and an increase in aggregated β-sheet. It may be concluded that large loops aggregate to give intermolecularly aggregated β-sheet, although this is

simultaneously formed from the other two components and a steady-state is reached with respect to its percentage.

The effect of the substrate MgATP on cat-ζ is very interesting because it induced changes in the secondary structure. In its presence there was an increase in the open large loops absorbing at 1648 cm^{-1}, and a considerable decrease in the 3_{10}-helix plus associated loops possibly indicating changes in the tertiary structure which may impede interaction between loops. Other changes included a decrease in the α-helix at 1658 cm^{-1} and an increase in the β-sheet at 1631 cm^{-1}. In addition, MgATP significantly altered the denaturation pattern of cat-ζ because it protected against denaturation, as revealed by the considerable shift in the onset of widening of the amide I′ band. It also changed the way in which the secondary structure was altered so that, whereas α-helix at 1655 cm^{-1} was preserved to a certain extent, the β-sheet component decreased to a greater extent than at 25 °C in the presence of MgATP. It is very interesting that significant differences in secondary structure were detected when PKB in an inactive form [42] (PDB code 1MRV) and PKB in a complex with AMPPNP and a substrate peptide [44] (PDB code 1O6K) were compared (Table 2). These differences confirmed the plasticity of these proteins and their capacity to change secondary structure as the result of interacting with substrates, as we observed here for PKCζ.

In summary, the secondary structure of cat-ζ, as observed by IR spectroscopy, is quite compatible with that revealed using high-resolution studies of catalytic domains from other analogous kinases. The structure is flexible, so that it is modulated by the presence of the substrate MgATP. During thermal unfolding 2D correlation spectroscopy reveals the way in which the different components transform from one into another, with open loops preceding the formation of aggregated β-sheets.

Experimental procedures

Materials

ATP was purchased from Roche Diagnostics (Barcelona, Spain). Deuterated water (D_2O) was purchased from Aldrich Chemical Co. (Milwaukee, WI). Pseudosubstrate inhibitor (sequence: H-Ser-Ile-Tyr-Arg-Arg-Gly-Ala-Arg-Arg-Trp-Arg-Lys-Leu-OH) was purchased from Calbiochem (La Jolla, CA). Water was twice distilled and deionized using a Millipore system from Millipore Ibérica (Madrid, Spain).

Expression and purification of cat-ζ

Rat PKCζ cDNA was a gift from Y. Nishizuka and Y. Ono (Kobe University, Kobe, Japan). The cDNA for PKCζ (229–592) was cloned into pFastBacHTb (Invitrogen, Barcelona, Spain) using the *Xho*I and *Kpn*I restriction sites, resulting in a fusion protein with N-terminal His-tag with TEV cleavage site. The recombinant viruses were obtained using standard procedures for transposition and transfection as indicated by the manufacturer (Invitrogen). Sf9 (*Spodoptera frugiperda*) insect cells were used. For expression, 2×10^6 Sf9 cells·mL^{-1} were infected with a high titre of recombinant baculovirus and the cells were harvested after 60 h incubation at 28 °C. Cells were resuspended in homogenization buffer (25 mM Tris/HCl, pH 8.0, 400 mM KCl, 0.25% Triton X-100, 10% glycerol, 10 mM benzamidine, 1 mM phenylmethanesulfonyl fluoride, 10 μg·mL^{-1} trypsin inhibitor, 4 μg·mL^{-1} pepstatine, 4 μg·mL^{-1} aprotinine and 10 μg·mL^{-1} leupeptin). The pellet was disrupted by sonication (6×10 s), and the resulting lysate was centrifuged at 100 000 ***g*** for 30 min. The supernatant was incubated for 1.5 h with Ni-beads, and the target protein was eluted with an elution buffer (25 mM Tris/HCl, pH 8.0, 200 mM NaCl and 0.5 mM dithiothreitol) containing increasing concentrations of imidazole. Most cat-ζ was eluted in 150 mM imidazole and loaded onto the Mono Q anion-exchange column (Mono Q 5/50 GL, Amersham Biosciences, Uppsala, Sweden) and eluted with an increasing salt concentration. The buffer system used was: (A) 20 mM Tris (pH 8.0), 200 mM NaCl, 5% glycerol, 0.5 mM dithiothreitol and (B) 20 mM Tris (pH 8.0), 5% glycerol, 0.5 mM dithiothreitol and 1 M NaCl. Fractions containing cat-ζ were pooled and loaded onto a Superdex-200 gel filtration column (Superdex 200 10/300 GL; Amersham Biosciences). Fractions corresponding to cat-ζ monomers were collected and concentrated up to 30 mg·mL^{-1} using an Ultrafree-30 centrifugal filter device (Millipore Inc., Bedford, MA) and the concentration was determined using the method described by Smith *et al*. [51]. The purity of the sample was checked by silver staining, and it was seen to be >95%.

Kinase activity assay

The kinase activity was measured by adding 25 ng of protein to the reaction mixture (final volume, 50 μL), which contained 25 mM Tris/HCl, pH 7.5, 0.1 mg·mL^{-1} peptide substrate, 100 μM [^{32}P]ATP[γP] (500 000 cpm·$nmol^{-1}$), 5 mM $MgCl_2$, 1 mM dithiothreitol and 0.5 mM EGTA. The reaction was started by the addition of 5 μL of the purified cat-ζ. After 10 min, the reaction was stopped with 1 mL of ice-cold 25% trichloroacetic acid and 1 mL of ice-cold 0.05% BSA. After precipitation on ice for 30 min, the protein precipitate was collected on a 2.5-cm glass filter and washed with 10 mL of ice-cold 10% trichloroacetic acid.

The amount of [$^{32}P_i$] incorporated into the peptide was measured using liquid scintillation counting. The linearity of the assay was confirmed from the time course of peptide phosphorylation over 15 min. The kinase activity measured for the isolated cat-ζ was 116 nmol $P_i \cdot min^{-1} \cdot mg^{-1}$ protein.

IR spectroscopy

Cat-ζ was prepared at 20 $mg \cdot mL^{-1}$ (420 μM) in H_2O buffer and at 5 $mg \cdot mL^{-1}$ (105 μM) in D_2O buffer, containing in both cases 20 mM Tris/HCl pH 8.0 (or pD 7.6), 200 mM NaCl, 1 mM dithiothreitol and 5 mM $MgCl_2$. When D_2O buffer was used, the protein was incubated overnight at 4 °C to maximize H–D exchange. To study the IR amide bands of the protein in the presence of MgATP, the protein was prepared in D_2O buffer and mixed with the protein to a final concentration of 1 mM.

IR spectra were recorded using a Bruker Vector 22 FTIR spectrometer equipped with an MCT detector. Samples were examined in a thermostated Specac 20710 cell (Specac, Orpington, UK) equipped with CaF_2 windows and 6 μm spacers (H_2O buffer) or 25 μm spacers (D_2O buffer). The spectra were recorded after equilibrating the samples at 25 °C for 20 min in the IR cell. A total of 128 scans were accomplished for each spectrum with a nominal resolution of 2 cm^{-1} and then Fourier transformed using a triangular apodization function. A sample shuttle accessory was used to obtain the average background and sample spectra. The sample chamber of the spectrometer was continuously purged with dry air to prevent atmospheric water vapour obscuring the bands of interest. Samples were scanned between 25 and 80 °C at 5 °C intervals with a 5 min delay between each scan using a circulation water bath interfaced to the spectrometer computer. IR spectroscopy of aqueous samples can be used to study protein structure thanks to spectral subtraction [52]. Spectral subtraction was performed interactively using the GRAMS/32 program (Galactic Industries Corporation, Salem, NH). Solvent contribution was eliminated by subtracting the pure buffer spectrum from the protein sample spectrum, in order to maintain a flat baseline between 2000 and 1300 cm^{-1}, as described previously [32]. This procedure eliminated any possible water contamination because the water band at 2150 cm^{-1} was abolished when using D_2O buffers [35]. In some experiments in which MgATP was also present at 1 mM concentration, it was necessary to subtract the spectrum of the buffer containing 1 mM MgATP from the spectrum containing protein also. The contribution of 1 mM ATP in the amide I before subtraction was < 3% of the total amide I area. In order to improve curve fitting, the spectra were then subjected to a baseline processing in the amide I or I′ regions (1700–1600 cm^{-1}), so that the extremes were rearranged to a zero-absorbance level by using the 'Adjust baseline' function of the GRAMS/32 program. Afterwards the spectra were processed by carrying out second-derivation according to Griffiths & Pariente [53], using GRAMS/32. Derivation gave the number and position, as well as an estimation of the bandwidth and the intensity of the bands making up the amide I or I′ region. Thereafter, curve fitting was performed and the heights, widths and positions of each band were optimized successively. Data treatment and band decomposition of the original amide I or amide I′ regions have been described previously [29,32,54]. The fractional areas of the bands in the amide I or amide I′ regions were calculated from the final fitted band areas. It is assumed that the extinction coefficients of the different protein components do not differ greatly and that, in any case, the error derived from this assumption is within the range of errors inherent to the method. The solution given by application of the computer programs to the decomposition of amide I band may not be the only one. Because some restrictions are imposed, for example maintenance of the initial band positions obtained from the second derivative in an interval of ± 1 cm^{-1}, preservation of bandwidth within the expected limits (typically 15–20 cm^{-1} in IR spectroscopy) and agreement with theoretical boundaries and predictions, the result is, in practice, unique.

The signal-to-noise ratio was calculated through the ratio of intensities between the maximum of the amide I or I′ band, at 1646 cm^{-1}, and the intensity at a frequency outside this region, where no significant absorbance takes place like, such as 1780 cm^{-1}. This was found to be ~600 in all the samples studied.

The procedure used here to quantitatively calculate the secondary structure is usually assumed to have an error of ~1% [29], and we assumed it to be 1–2%, as deduced from the comparison of at least three independent experiments and the repetition of the fitting procedure by three different persons. We therefore regard as significant changes in the structural components that are > 3%.

Difference spectra were obtained by subtracting two absorption spectra using a factor that resulted in the 1700–1600 cm^{-1} interval (amide I) having identical positive and negative area.

2D correlation analysis was carried out using the 2D-POCHA program written by D. Adachi and Y. Ozaki (Kwansei Gakuin University, Japan), which can be found at the following website: http://science.kwansei.ac.jp/~ozaki/2D-Pocha.htm. This software can calculate the 2D correlation spectroscopy proposed by I. Noda [37,55]. The maximum intensity of the whole correlation map is divided by six, giving a contour map in which the main peak, i.e. the one with the maximum intensity, will be surrounded by six contour lines, whereas the rest of the peaks will show a number of contour lines reflecting their intensities in relation to the main peak. As reviewed by Noda [37,55], the synchronous 2D correlation spectrum of dynamic spectral intensity variations represents the simultaneous occurrence of coincidental changes in spectral intensities measured at ν_1 and ν_2. Correlation peaks appear at both diagonal (auto-

peaks) and off-diagonal peaks (cross-peaks). The asynchronous spectrum of dynamic spectral intensity variations represents sequential, or unsynchronized, changes in spectral intensities measured at ν_1 and ν_2. The asynchronous spectrum has no autopeaks, but consists entirely of cross-peaks located at off-diagonal positions. An asynchronous cross-peak develops only if the intensities of two dynamic spectral intensities vary out of phase with each other for some Fourier-frequency components of signal fluctuations. Depending on the signal of a given cross-peak in the asynchronous map and on the corresponding region of the synchronous map, the order of changes in the correlated wavenumbers, ν_1 and ν_2, can be defined [54]. In this way, if $\nu_1 > \nu_2$, the cross-peak (ν_1, ν_2) is positive in the asynchronous map and the corresponding region of the synchronous map is also positive, then the change in ν_1 precedes the change in ν_2. However, if the corresponding region of the synchronous map is negative, then changes in ν_2 occur before changes in ν_1. This rule is reversed if $\nu_1 > \nu_2$.

Acknowledgements

This work was supported by grants BFU2005-02482 from the Dirección General de Investigación, Ministerio de Educación y Ciencia (Spain) and 00591/PI/04 from the Fundación Séneca (Comunidad Autónoma de Murcia, Spain). SSB is the recipient of a fellowship from the Ministerio de Educación y Ciencia (Spain). AK and MB were Marie Curie postdoctoral Fellows (European Commission). AT is the recipient of a postdoctoral fellowship from the Universidad de Murcia. SC-G belongs to the Ramón y Cajal Programme supported by Ministerio de Ciencia y Tecnolog'a and Universidad de Murcia. Rat PKCζ cDNA was a kind gift from Drs Nishizuka and Ono (Kobe University, Kobe, Japan).

References

1 Hofmann J (1994) Protein kinase C isozymes as potential targets for anticancer therapy. *Curr Cancer Drug Targets* **4**, 125–146.
2 Mackay HJ & Twelves CJ (2003) Protein kinase C: a target for anticancer drugs? *Endocrin Relat Cancer* **10**, 389–396.
3 Mellor H & Parker PJ (1998) The extended protein kinase C superfamily. *Biochem J* **332**, 281–292.
4 Newton AC (2001) Protein kinase C: structural and spatial regulation by phosphorylation, cofactors, and macromolecular interactions. *Chem Rev* **101**, 2353–2364.
5 Nakanishi H, Brewer KA & Exton JH (1993) Activation of the ζ isozyme of protein kinase C by phosphatidylinositol 3,4,5-trisphosphate. *J Biol Chem* **268**, 13–16.
6 Standaert ML, Bandyopadhyay G, Kanoh Y, Sajan MP & Farese RV (2001) Insulin and PIP_3 activate PKC-zeta by mechanisms that are both dependent and independent of phosphorylation of activation loop (T410) and autophosphorylation (T560) sites. *Biochemistry* **40**, 249–255.
7 Muller G, Ayoub M, Storz P, Rennecke J, Fabbro D & Pfizenmaier K (1995) PKCζ is a molecular switch in signal transduction of TNF-α, bifunctionally regulated by ceramide and arachidonic acid. *EMBO J* **14**, 1961–1969.
8 Limatola C, Schaap D, Moolenaar WH & van Blitterswijk WJ (1994) Phosphatidic acid activation of protein kinase C-ζ overexpressed in COS cells: comparison with other protein kinase C isotypes and other acidic lipids. *Biochem J* **304**, 1001–1008.
9 Chou MM, Hou W, Johnson J, Graham LK, Lee MH, Chen C-S, Newton AC, Schaffhausen BS & Toker A (1998) Regulation of protein kinase C ζ by PI 3-kinase and PDK-1. *Curr Biol* **8**, 1069–1077.
10 Le Good JA, Ziegler WH, Parekh DB, Alessi DR, Cohen P & Parker PJ (1998) Protein kinase C isotypes controlled by phosphoinositide 3-kinase through the protein kinase PDK1. *Science* **281**, 2042–2045.
11 Hirai T & Chida K (2003) Protein kinase Cζ (PKCζ): activation mechanisms and cellular functions. *J Biochem (Tokyo)* **133**, 1–7.
12 Kampfer S, Hellbert K, Villunger A, Doppler W, Baier G, Grunicke HH & Uberall F (1998) Transcriptional activation of c-fos by oncogenic Ha-Ras in mouse mammary epithelial cells requires the combined activities of PKC-lambda, epsilon and zeta. *EMBO J* **15**, 4046–4055.
13 Selbie LA, Schmitz-Peiffer C, Sheng Y & Biden TJ (1993) Molecular cloning and characterization of PKC iota, an atypical isoform of protein kinase C derived from insulin-secreting cells. *J Biol Chem* **15**, 24296–24302.
14 Tabuse Y, Izumi Y, Piano F, Kemphues KJ, Miwa. J & Ohno S (1998) Atypical protein kinase C cooperates with PAR-3 to establish embryonic polarity in *Caenorhabditis elegans*. *Development* **125**, 3607–3614.
15 Sanz L, Sánchez P, Lallena MJ, Diaz-Meco MT & Moscat J (1999) The interaction of p62 with RIP links the atypical PKCs to NF-kappaß activation. *EMBO J* **18**, 3044–3053.
16 Cohen P (2002) Protein kinases – the major drug targets of the twenty-first century? *Nat Rev Drug Discov* **1**, 309–315.
17 Moscat J & Díaz-Meco MT (2000) The atypical protein kinase Cs. Functional specificity mediated by specific protein adapters. *EMBO Report* **1**, 399–403.
18 Messerschmidt A, Macieira S, Velarde M, Bädeker M, Benda C, Jestel A, Brandstetter H, Neuefeind T & Blaesse M (2005) Crystal structure of the catalytic domain of human atypical protein kinase C-iota reveals

interaction mode of phosphorylation site in turn motif. *J Mol Biol* **352**, 918–931.
19 Xu ZB, Chaudhary D, Olland S, Wolfrom S, Czerwinski R, Malakian K, Lin L, Stahl ML, Joseph-McCarthy D, Benander C *et al.* (2004) Catalytic domain crystal structure of protein kinase C-θ (PKCθ). *J Biol Chem* **279**, 50401–50409.
20 Arrondo JLR & Goñi FM (1999) Structure and dynamics of membrane proteins as studied by infrared spectroscopy. *Prog Biophys Mol Biol* **72**, 367–405.
21 Bandekar J & Krimm S (1980) Vibrational analysis of peptides, polypeptides, and proteins. VI. Assignment of beta-turn modes in insulin and other proteins. *Biopolymers* **19**, 31–36.
22 Bandekar J (1992) Amide modes and protein conformation. *Biochim Biophys Acta* **1120**, 123–143.
23 Fabian H, Naumann D, Misselwitz R, Ristau O, Gerlach D & Welfle H (1992) Secondary structure of streptokinase in aqueous solution: a Fourier transform infrared spectroscopic study. *Biochemistry* **31**, 6532–6538.
24 Alvarez J, Haris PI, Lee DC & Chapman D (1987) Conformational changes in concanavalin A associated with demetallization and alpha-methylmannose binding studied by Fourier transform infrared spectroscopy. *Biochim Biophys Acta* **916**, 5–12.
25 Arrondo JL, Young NM & Mantsch HH (1988) The solution structure of concanavalin A probed by FT-IR spectroscopy. *Biochim Biophys Acta* **952**, 261–268.
26 Arrondo JLR, Blanco FJ, Serrano L & Goñi FM (1996) Infrared evidence of a β-hairpin peptide structure in solution. *FEBS Lett* **384**, 35–37.
27 Saba RI, Ruyschaert JM, Herschuelz A & Goormaghtigh E (1999) Fourier transform infrared spectroscopy study of the secondary and tertiary structure of the reconstituted Na^+/Ca^{2+} exchanger 70-kDa polypeptide. *J Biol Chem* **274**, 15510–15518.
28 Hadden JM, Bloemendal M, Haris P, Srai SKS & Chapman D (1994) Fourier transform infrared spectroscopy and differential scanning calorimetry of transferrins: human serum transferrin, rabbit serum transferrin and human lactoferrin. *Biochim Biophys Acta* **1205**, 59–67.
29 Arrondo JLR, Castresana J, Valpuesta JM & Goñi FM (1994) Structure and thermal denaturation of crystalline and noncrystalline cytochrome oxidase as studied by infrared spectroscopy. *Biochemistry* **33**, 11650–11655.
30 Krimm S & Bandekar J (1986) Vibrational spectroscopy and conformation of peptides, polypeptides, and proteins. *Adv Protein Chem* **38**, 181–364.
31 Fraser RDB & MacRae TP (1973) *Conformation in Fibrous Protein and Related Synthetic Polypeptides*. Academic Press, New York.
32 Arrondo JLR, Muga A, Castresana J, Bernabeu C & Goñi FM (1989) An infrared spectroscopic study of β-galactosidase structure in aqueous solutions. *FEBS Lett* **252**, 118–120.
33 Shimanouchi T, Tsuboi M & Kyogoku Y (1964) Infrared spectra of nucleic acids. In *Advances in Chemical Physics* (Duchesne J, ed.), pp. 435–498. Wiley Interscience, New York.
34 Surewicz WK, Leddy JJ & Mantsch HH (1990) Determination of protein secondary structure by Fourier transform infrared spectroscopy: a critical assessment. *Biochemistry* **29**, 8106–8111.
35 Powell JR, Wasacz FM & Jakobsen RJ (1986) An algorithm for the reproducible spectral subtraction of water from the FT-IR spectra of proteins in dilute solutions and adsorbed monolayers. *Appl Spectrosc* **40**, 339–344.
36 Susi H (1972) Infrared spectroscopy-conformation. *Methods Enzymol* **26**, 455–472.
37 Noda I (1989) Two-dimensional infrared spectroscopy. *J Am Chem Soc* **111**, 8116–8118.
38 Torrecillas A, Corbalán-García S & Gómez-Fernández JC (2003) Structural study of the C2 domains of the classical PKC isoenzymes using infrared spectroscopy and two-dimensional infrared correlation spectroscopy. *Biochemistry* **42**, 11669–11681.
39 Torrecillas A, Corbalán-García S & Gómez-Fernández JC (2004) An infrared spectroscopic study of the secondary structure of protein kinase C alpha and its thermal denaturation. *Biochemistry* **43**, 2332–2344.
40 Arrondo JLR, Iloro I, Aguirre J & Goñi FM (2004) A two-dimensional IR spectroscopic (2D-IR) simulation of protein conformational changes. *Spectrosc Int J* **18**, 49–58.
41 Akamine P, Madhusudan Wu J, Xuong NH, Ten Eyck LF & Taylor SS (2003) Dynamic features of cAMP-dependent protein kinase revealed by apoenzyme crystal structure. *J Mol Biol* **14**, 159–171.
42 Huang X, Begley M, Morgenstern KA, Gu Y, Rose P, Zhao H & Zhu X (2003) Crystal structure of an inactive Akt2 kinase domain. *Structure (Camb)* **11**, 21–30.
43 Manning G, Whyte DB, Martinez R, Hunter T & Sudarsanam S (2002) The protein kinase complement of the human genome. *Science* **298**, 1912–1934.
44 Yang J, Cron P, Good VM, Thompson V, Hemmings BA & Barford D (2002) Crystal structure of an activated Akt/protein kinase B ternary complex with GSK3-peptide and AMP-PNP. *Nat Struct Biol* **9**, 940–944.
45 Holloway PW & Mantsch HH (1989) Structure of cytochrome b_5 in solution by Fourier-transform infrared spectroscopy. *Biochemistry* **28**, 931–935.
46 Prestrelski SJ, Byler DM & Thompson MP (1991) Infrared spectroscopic discrimination between alpha- and 3(10)-helices in globular proteins. Reexamination of amide I infrared bands of alpha-lactalbumin and their assignment to secondary structures. *Int J Pept Protein Res* **37**, 508–512.

47 Miick SM, Martinez GV, Fiori WR, Todd AP & Millhauser GL (1992) Short alanine-based peptides may form 3(10)-helices and not alpha-helices in aqueous solution. *Nature* **359**, 653–655.
48 Mouro C, Jung C, Bodon A & Simonneaux G (1997) Comparative Fourier transform infrared studies of the secondary structure and the CO heme ligand environment in cytochrome P-450cam and cytochrome P-420cam. *Biochemistry* **36**, 8125–8134.
49 De las Rivas J & Barber J (1997) Structure and termal stability of photosystem II reaction centres studied by infrared spectroscopy. *Biochemistry* **36**, 8897–8903.
50 Gorne-Tschelnow Naumann D, Weise C & Hucho F (1993) Secondary structure behaviour of acetylcholinesterase. Studies by Fourier-transform infrared spectroscopy. *Eur J Biochem* **213**, 1235–1242.
51 Smith PK, Krohn RI, Hermanson GT, Mallia AK, Gartner FH, Provenzano MD, Fujimoto EK, Goeke NM, Olson BJ & Klenk DC (1985) Measurement of protein using bicinchoninic acid. *Anal Biochem* **150**, 76–85.
52 Chapman D, Gomez-Fernandez JC, Goni FM & Barnard M (1980) Difference infrared spectroscopy of aqueous model and biological membranes using an infrared data station. *J Biochem Biophys Methods* **2**, 315–323.
53 Griffiths PR & Pariente G (1986) Introduction to spectral deconvolution. *Trends Anal Chem* **5**, 209–215.
54 García-García J, Corbalán-García S & Gómez-Fernández JC (1999) Effect of calcium and phosphatidic acid binding on the C2 domain of PKC alpha as studied by Fourier transform infrared spectroscopy. *Biochemistry* **38**, 9667–9675.
55 Noda I (1993) Generalized two-dimensional correlation method applicable to infrared, Raman, and other types of spectroscopy. *Appl Spectrosc* **47**, 1329–1336.